Int. J. Multiphase Flow Vol. 19, No. 1, pp. 79–89, 1993
Printed in Great Britain

0301-9322/93 $6.00 + 0.00
Pergamon Press Ltd

BEHAVIOR OF LIQUID FILMS AND DROPLETS IN THE NON-EQUILIBRIUM REGION OF A DOWNWARD ANNULAR MIST FLOW (COMPARISON OF POROUS AND CENTRAL NOZZLE MIXING METHODS)

O. OKADA[1] and H. FUJITA[2]

[1]Department of Mechanical Engineering, Suzuka College of Technology, Shirokocho, Suzuka, Mie 510-02, Japan

[2]Department of Mechanical Engineering, Nagoya University, Furocho, Chikusaku, Nagoya 464-01, Japan

(Received 25 June 1991; in revised form 25 August 1992)

Abstract—Experiments were conducted on the behavior of liquid films and droplets in the non-equilibrium region of a downward annular mist flow, using a vertical pipe of about 30 mm dia and 6.5 m long, under two extreme conditions of air–water mixing with either a porous wall or a central nozzle to feed the water. The onset of large disturbance waves was influenced remarkably by the mixing method. Axial changes in the film thickness, wave velocity and frequency were obtained by the electrical conductivity method. The water droplet mass flux distributions were measured by an isokinetic sampling probe. In porous wall mixing, large disturbance waves occurred farther upstream than in nozzle mixing. The fraction of liquid-entrained E axially increased monotonously and attained a certain constant value, whereas in nozzle mixing it decreased monotonously and became constant. For high air velocity and high water velocity, the non-equilibrium length $(z/d)_E$ was 70–140. The critical liquid film thickness depended heavily on the gas velocity in a downward annular mist flow in contrast with an upward flow.

Key Words: annular mist flow, non-equilibrium length, disturbance waves, liquid film thickness, liquid droplets, wave velocity, frequency

1. INTRODUCTION

Two-phase flow phenomena in actual devices are often in non-equilibrium. Therefore, it is necessary to accumulate and analyze the fundamental data on the flow in non-equilibrium in order to improve performance and assure the safety of instruments connected with such flow. However, there have been only a few systematic studies on the flow in a non-equilibrium region (Webb 1970; Okada & Fujita 1990).

Experiments were conducted on the behavior of liquid films and droplets in the non-equilibrium region of a downward annular mist flow, using a vertical pipe of about 30 mm dia and 6.5 m long, under the two extreme conditions of air–water mixing using either a porous wall or a central nozzle equipped to supply water along the pipe axis.

The liquid film formation and the onset of large disturbance waves (LDW) were observed to be influenced remarkably by the mixing method. Axial changes of the water film characteristics in relation to the dispersed liquid droplets (i.e. the film thickness, wave velocity and frequency) were obtained by the electrical conductivity method. The water droplet mass flux distributions were measured by an isokinetic sampling probe. On the basis of these results, the non-equilibrium length was discussed for both mixing methods.

2. EXPERIMENTAL APPARATUS AND PROCEDURE

A schematic diagram of the experimental apparatus is shown in figure 1. A transparent acrylic test pipe TS_1 (dia $d = 29.57$ mm, length $l = 6.20$ m) was made available to measure various properties of the liquid film and to observe flow patterns. Electrodes to measure the behavior of liquid film by the electrical conductivity method were placed at C_1–C_{20} ($z/d = 6.7$ to 196.7) on TS_1, arranged at 300 mm intervals in the axial direction, where z is the axial distance from the mixing device. Each platinum electrode (0.75 mm dia, 15 mm long), as shown in figure 2, was installed flush

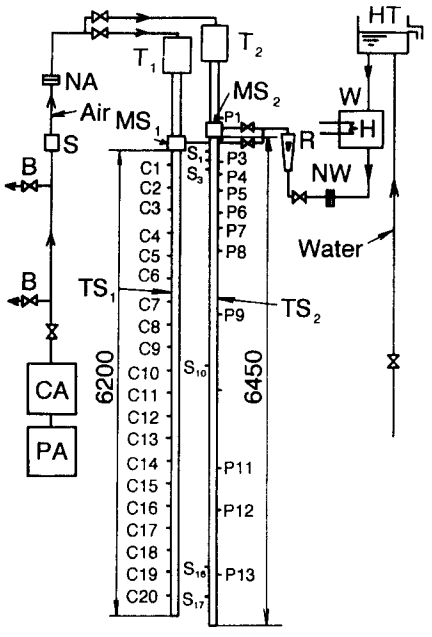

Figure 1. Schematic diagram of the experimental apparatus.

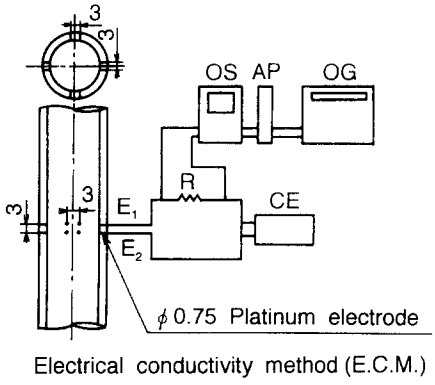

Figure 2. Electrode circuitry for measuring the liquid film.

with the inner surface of the pipe in a 3-mm square arrangement, at four sites on the periphery of the same cross section. The total number of electrodes was 320 in 20 cross sections.

A brass pipe TS_2 ($d = 29.87$ mm, $l = 6.45$ m) was used to measure the pressure loss and the entrained water mass flux distribution; P_1–P_{13} denote the positions of the pressure taps used to measure the static pressure at each cross section. The pressure difference of the adjacent section was measured with an aqueous monometer. S_1–S_{17} denote the positions of the holes for inserting an isokinetic sampling probe; these holes were plugged flush with the pipe wall when not in use.

Compressed air from air compressor PA was passed through a quadrant-edge nozzle NA, an air calming tank T_1 or T_2, a honeycomb, a bellmouth and a pipe which was longer than the inlet length; it then entered a device for mixing air and water MS_1 or MS_2 (see figure 1).

Water fed from a constant head tank HT passed through a tank for controlling the water temperature W, then the quadrant-edge nozzle NW and finally entered the mixing device.

In order to compare the influence of the air–water mixing method on the flow characteristics, two extreme cases of porous wall mixing and central nozzle mixing were adopted (figure 3). For porous wall mixing, a sintered porous section of the pipe (31 mm i.d. 25 mm long, 40 μm magnitude of voids) was incorporated as a test pipe component in the mixing chamber. For nozzle mixing, a stainless steel tube 3.0 mm dia was equipped with a stay in the center of the pipe.

Annular mist flow was formed behind the mixing device. The nozzle exit or the end of the porous wall was set as the origin with an axial distance z. The entrained water mass flux distribution was measured by an isokinetic probe (shown in figure 4), whose outer and inner diameters were 3.0 and 1.2 mm, respectively. The rate of entrained water droplets was obtained by measuring the

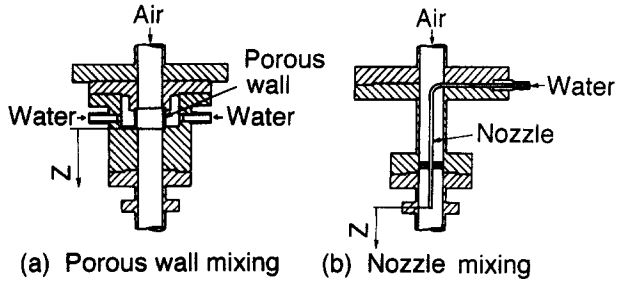

Figure 3. Air–water mixing device: (a) porous wall mixing; (b) nozzle mixing.

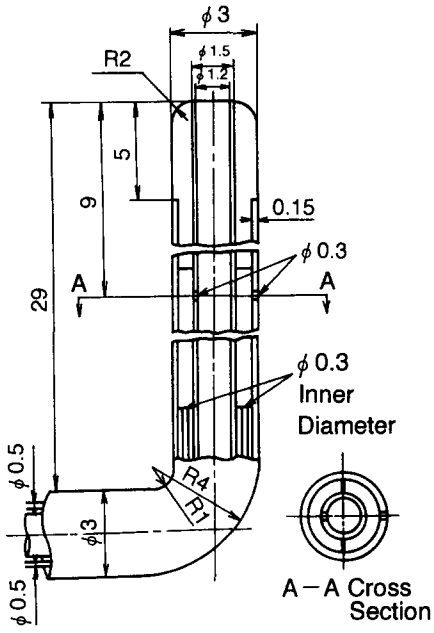

Figure 4. Isokinetic sampling probe.

weight of a collector connected to the isokinetic probe for 3–5 min to an accuracy within 1 mg. The experimental error for the liquid entrainment measurement is, at most, ±6%.

Experiments were performed at various air and water flow rates (see table 1). The present experiment covers a comparatively lower water rate and a higher air velocity; wherein the apparent gas velocity $u_{G0} = 18.0$ to 87.0 m/s (measured just upstream of the mixing device; "apparent" is omitted hereafter), the gas Reynolds number $Re_{G0} = 3.6 \times 10^4$ to 2.1×10^5, the liquid velocity $u_{L0} = 4.86 \times 10^{-3}$ to 5.34×10^{-2} m/s and the liquid Reynolds number $Re_{L0} = 179$ to 1971; the air and water temperatures were kept equal in the range 20–30°C.

3. EXPERIMENTAL RESULTS AND DISCUSSION

3.1. Flow regime

The changes in the flow pattern and flow regime were observed to elucidate the process by which the two-phase flow developed. Figure 5 shows a flow regime map measured in an equilibrium region at the position $z/d = 180$. The experimental results in vertical upward flow from Sekoguchi *et al.* (1973) and Nedderman & Shearer (1963) are presented in figure 5. The present flow regime coincides with those of Sekoguchi *et al.* and Nedderman & Shearer, except for the case of low u_{G0}.

Table 1. Experimental conditions

Air		Water			
u_{G0} (m/s)	Re_{G0}	u_{L0} (m/s)	Re_{L0}	u_{L0} (m/s)	Re_{L0}
18.0	3.6×10^4	4.86×10^{-3}	179	2.67×10^{-2}	986
27.5	5.5×10^4	7.30×10^{-3}	269	2.92×10^{-2}	1075
36.0	7.5×10^4	9.72×10^{-3}	358	3.16×10^{-2}	1165
44.0	9.6×10^4	1.22×10^{-2}	448	3.40×10^{-2}	1294
53.2	1.1×10^5	1.46×10^{-2}	538	3.65×10^{-2}	1344
61.6	1.4×10^5	1.70×10^{-2}	627	3.89×10^{-2}	1434
65.7	1.5×10^5	1.94×10^{-2}	717	4.13×10^{-2}	1523
70.0	1.6×10^5	2.19×10^{-2}	806	4.37×10^{-2}	1613
77.9	1.9×10^5	2.21×10^{-2}	813	4.62×10^{-2}	1702
87.0	2.1×10^5	2.43×10^{-2}	896	4.86×10^{-2}	1792
				5.10×10^{-2}	1882
				5.34×10^{-2}	1971

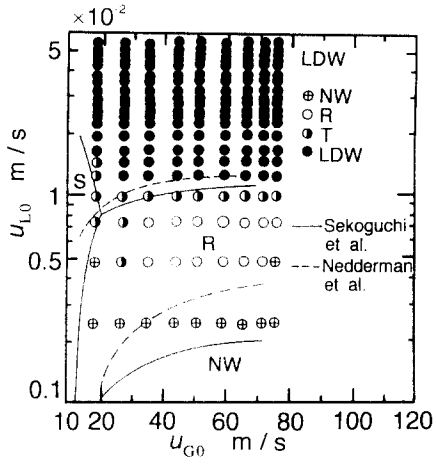

Figure 5. Flow regime map: NW, non-wetted region; R, ripple region; S, suspending wave region; LDW, large disturbance wave region.

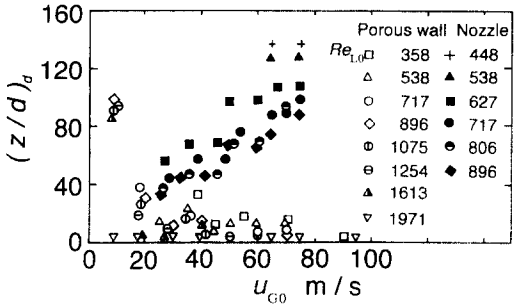

Figure 6. Points of inception of LDW.

3.2. *Inception of large disturbance waves (LDW)*

Since LDW are closely connected with the occurrence of entrained water droplets, the position of the LDW inception is very important in clarifying the developmental process of an annular mist flow. Quantitative definitions of LDW have been attempted by Sakaguchi *et al.* (1979), Sekoguchi *et al.* (1983) and Fukano *et al.* (1987). In this paper, LDW are simply defined as ones whose wave

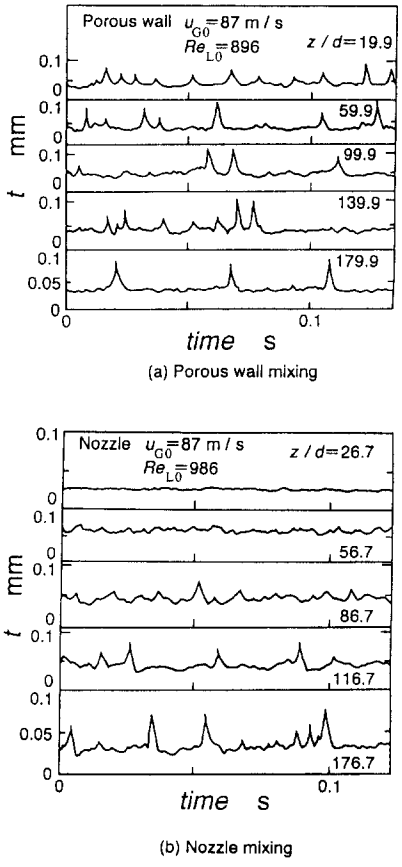

Figure 7. Typical traces of liquid film thickness in the non-equilibrium region by the electrical conductivity method.

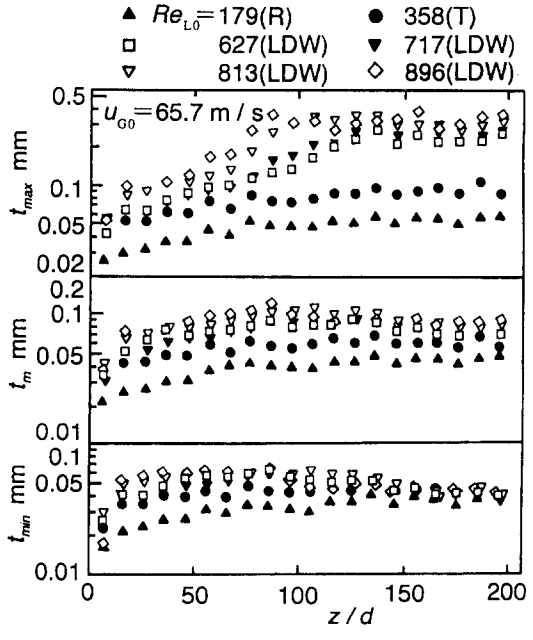

Figure 8. Axial change of the liquid film thickness (nozzle mixing): R, ripple; T, transient wave; LDW, large disturbance wave.

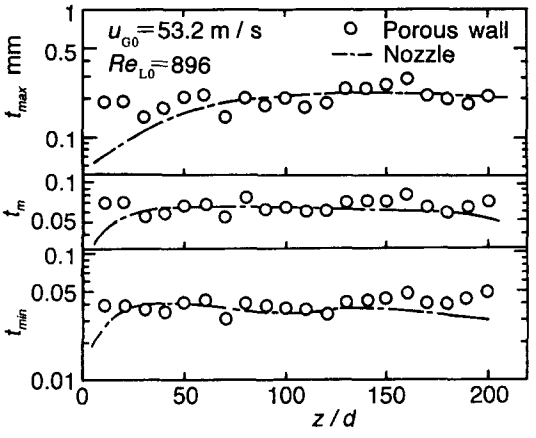

Figure 9. Axial change of the liquid film thickness in both mixing methods.

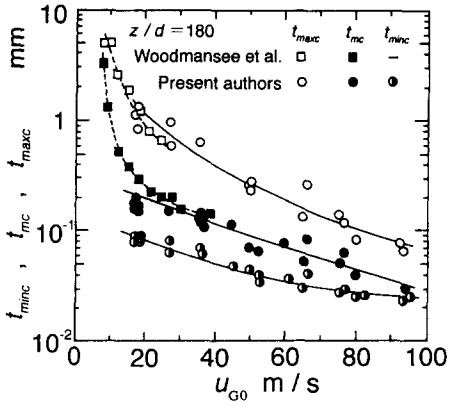

Figure 10. Critical liquid film thickness.

velocity is faster than in the ripple waves, usually forming a complete ring in the pipe and having a characteristically milky appearance.

Figure 6 shows the points of LDW inception $(z/d)_d$ vs u_{G0} and u_{L0}, both by gross observation and by using the wave output in the electrical conductivity method. It is clear that there is a great difference in $(z/d)_d$ with each of the mixing methods. In nozzle mixing, the points shifted more downstream as u_{G0} increased at fixed Re_{L0}. On the other hand, in porous wall mixing, LDW appeared farther upstream than for nozzle mixing, since the water film was formed immediately after the gas–liquid mixing. The points of LDW inception $(z/d)_d$ tend to move farther upstream, in contrast with nozzle mixing, as u_{G0} increases.

The influence of the water rate on $(z/d)_d$ has the same tendency in both mixing methods, and the value of $(z/d)_d$ decreased as Re_{L0} increased. The fact that LDW in porous wall mixing occurred farther upstream than in nozzle mixing is because a certain liquid film flow rate is necessary for LDW to occur. Accordingly, in nozzle mixing a longer inlet length is necessary for the dispersed water droplets to deposit and to form a water film on the pipe wall.

3.3. Liquid film thickness

Figure 7 shows typical traces of liquid film thickness in the non-equilibrium region by the electrical conductivity method. Observation of the change of wave motion of an annular film flow shows that ripples occur in the first instance, and LDW begin to occur after forming transitional flows in the flow direction.

Figure 8 shows an example of the axial change in the liquid film thickness at $u_{G0} = 65.7$ m/s, where t_{max}, t_m and t_{min} mean maximum, mean and minimum film thickness, respectively. Firstly, t_{min} becomes constant, gradually increasing in the axial direction at $Re_{L0} = 179$, where only ripples exist. At $Re_{L0} \geqslant 627$, where LDW appear, t_{min} first increases abruptly in the axial direction and then decreases after attaining a maximum value at a certain point. This decreasing tendency becomes

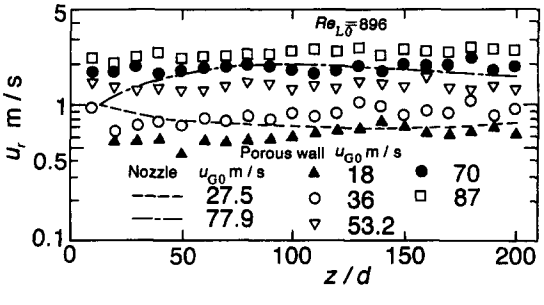

Figure 11. Axial change of the ripple velocity.

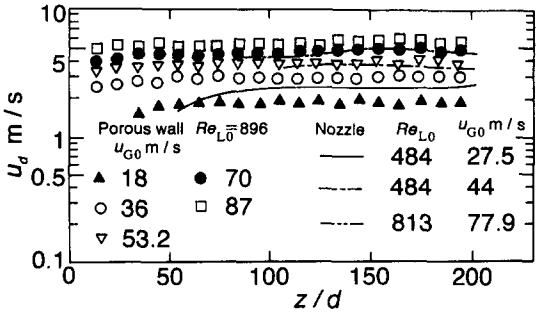

Figure 12. Axial change of LDW velocity.

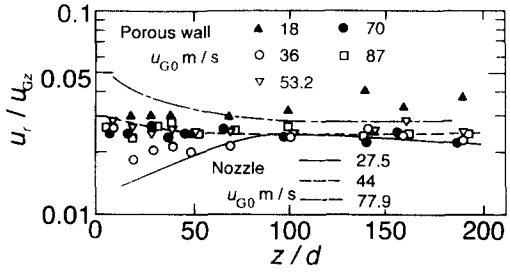

Figure 13. Axial change of u_r/u_{Gz} ($Re_{L0} = 896$).

remarkable as the air velocity increases. It is thought that the air velocity increases considerably in the flow direction due to the change in the air density resulting from the pressure loss. Secondly, t_m in the axial direction tends to be almost the same as for t_{min}; t_m naturally increases as Re_{L0} increases.

Thirdly, a remarkable difference in t_{max} is recognized between $Re_{L0} \leqslant 358$, where there is no LDW, and $Re_{L0} \geqslant 627$, where such waves exist. In the case of $Re_{L0} \leqslant 358$, t_{max} tends to be similar to t_{min} and t_m. On the other hand, for $Re_{L0} \geqslant 627$, t_{max} increases gradually at first in the axial direction and begins to increase abruptly at the point where t_{min} has the maximum value. This point virtually corresponds to the inception point of LDW. Then, t_{max} gradually begins to decrease in the axial direction.

Figure 9 shows the axial change of the liquid film thickness in both mixing methods. In porous wall mixing, t_{max}, t_m and t_{min} do not display a remarkable change in the axial direction. On the other hand, in nozzle mixing each film thickness increases gradually in the axial direction for $z/d < 50$. For $z/d \geqslant 50$, no difference in the liquid film tendency is observed with either mixing method.

At $u_{G0} = 87$ m/s, t_{max} and t_m tend to decrease gradually in the axial direction in porous wall mixing, while t_{min} does not change remarkably. In nozzle mixing, the axial position where t_{max} becomes constant shifts more downstream than at $u_{G0} = 53.2$ m/s. This well coincides with the result that the inception points of the LDW shift more downstream as u_{G0} increases as mentioned in section 3.2.

At a constant air velocity, the liquid film thickness generally increases as the water rate increases. But in the case of downward annular mist flow the thickness increases less and tends to approach a certain constant value, no matter how the water rate increases. In other words, the liquid film thickness has a critical value, independent of the water rate, and is heavily dependent on the air velocity.

Figure 10 shows the critical film thickness of t_{maxc}, t_{mc} and t_{minc}, depending on the air velocity u_{G0} at $z/d = 180$. For each film thickness, the experimental results are clustered along a curve, suggesting that the critical liquid film thickness is determined by u_{G0}. For $u_{G0} \geqslant 80$ m/s, where the air velocity is very great, even t_{maxc} becomes a very thin film which is <0.1 mm thick. In such a flow condition, where the wave height falls so much, the difference between ripples and LDW is thought to become less. Thus, it is the comparatively low air velocity region, rather than the high air velocity region, in which the inception of LDW has a remarkable influence on the liquid film flow characteristics. The experimental results in a horizontal duct by Woodmansee & Hanratty

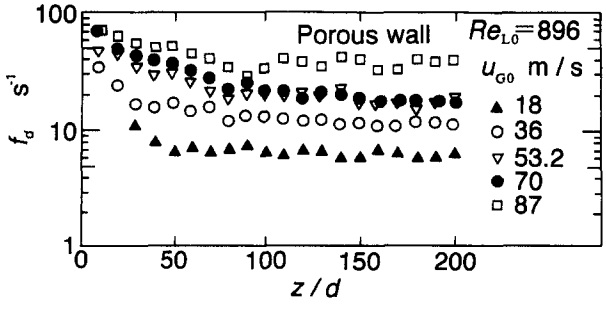

Figure 14. Axial change in the frequency of LDW.

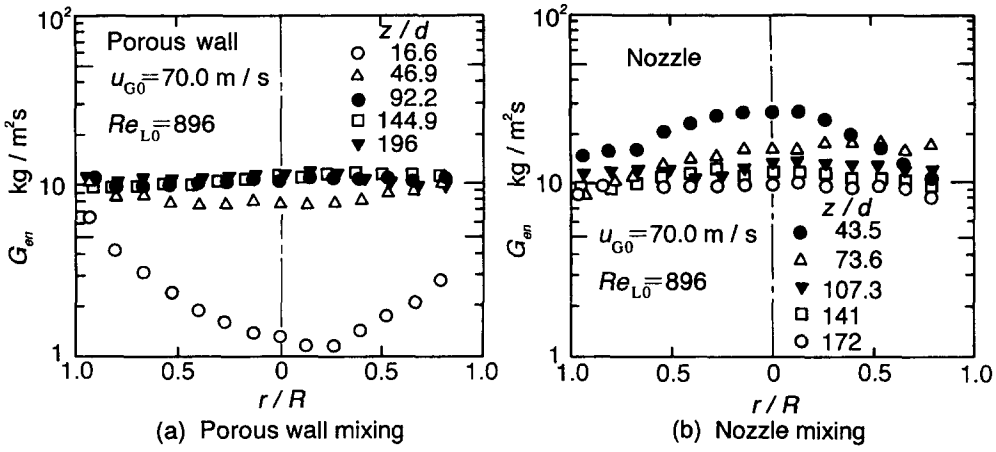

Figure 15. Axial change of the entrained water mass flux G_{en}: (a) porous wall mixing; (b) nozzle mixing.

(1969), included in the figure, coincide approximately with the extrapolation lines in the present experiment.

3.4. *Wave velocity and wave frequency*

We measured the velocity of ripples u_r from the signals obtained from two conductance electrodes located 3 mm apart in the axial direction, as mentioned in section 2, using the same techniques as in previous work (Takahama *et al.* 1983). Figure 11 shows the axial change of u_r in both mixing methods. In porous wall mixing a remarkable change of u_r is not evident, whereas in nozzle mixing the axial change of u_r depends considerably on the air velocity u_{G0}. When u_{G0} is low, u_r decreases in the axial direction and then approaches a constant value; when u_{G0} is high, on the other hand, u_r increases. But at $z/d \geqslant 100$, virtually no difference between them is apparent.

As shown in figure 12, the velocity of LDW u_d is 2–5.5 m/s. This is much larger than that of u_r; u_d increases slightly and monotonously in the axial direction with both mixing methods. The values of u_r and u_d tend to increase in the axial direction because the pressure in the pipe decreases and the air velocity increases due to the change of air density. This agrees almost qualitatively with Webb's (1970) experiment. Furthermore, u_d is heavily u_{G0} dependent: increasing as u_{G0} increases and increasing slightly as Re_{L0} increases. The increment of u_{G0} due to the change of air density in the axial direction becomes more remarkable at a higher air velocity. Thus, an example of the axial change of u_r/u_{Gz} is shown in figure 13, where u_{Gz} is the mean air velocity considering the air expansion at each cross section of the pipe. In porous wall mixing, no particularly remarkable change of u_r/u_{Gz} is recognized in the axial direction. In nozzle mixing, since u_r also depends on the liquid film thickness, the value of u_r/u_{Gz} shows the reverse trend, depending on whether u_{G0} is high or not, at $z/d < 100$. At $z/d \geqslant 100$, the influence of the mixing methods and u_{G0} on u_r/u_{Gz} becomes less. Further, the value of u_d/u_{Gz} is about 0.06–0.1 in both mixing methods and does not change in the axial direction. The more u_{G0} increases, the lower u_d/u_{Gz} becomes. An axial change in the wave frequency component involving LDW was recognized only rarely and frequency components, such as 200–600 Hz, increased slightly with z/d in both mixing methods.

Figure 14 shows an axial change in the frequency f_d of LDW in porous wall mixing. f_d abruptly decreases for $z/d \leqslant 50$, at $u_{G0} = 18.0$ m/s. At $u_{G0} = 87.0$ m/s, the range where f_d abruptly decreases grows to 90 d. It is also recognized in nozzle mixing that f_d decreases in the axial direction. Accordingly, it is thought that the coalescence of LDW and the liquid entrainment from those waves tend to increase. In addition, f_d increases with u_{G0} and Re_{L0}. This fact suggests that the increment of u_{G0} and Re_{L0} has a close relation to the increase in E. Therefore, f_d is also closely connected with E, as mentioned below.

Recently, Jayanti & Hewitt (1991) reported a new conceptual picture of the gas–liquid interface: the liquid film was found to contain a significant amount of air bubbles, which were continuously entrained, broken up and released by the rolling motion within the film. Their novel flow visualization experiments using the refractive index matching technique may change some aspect

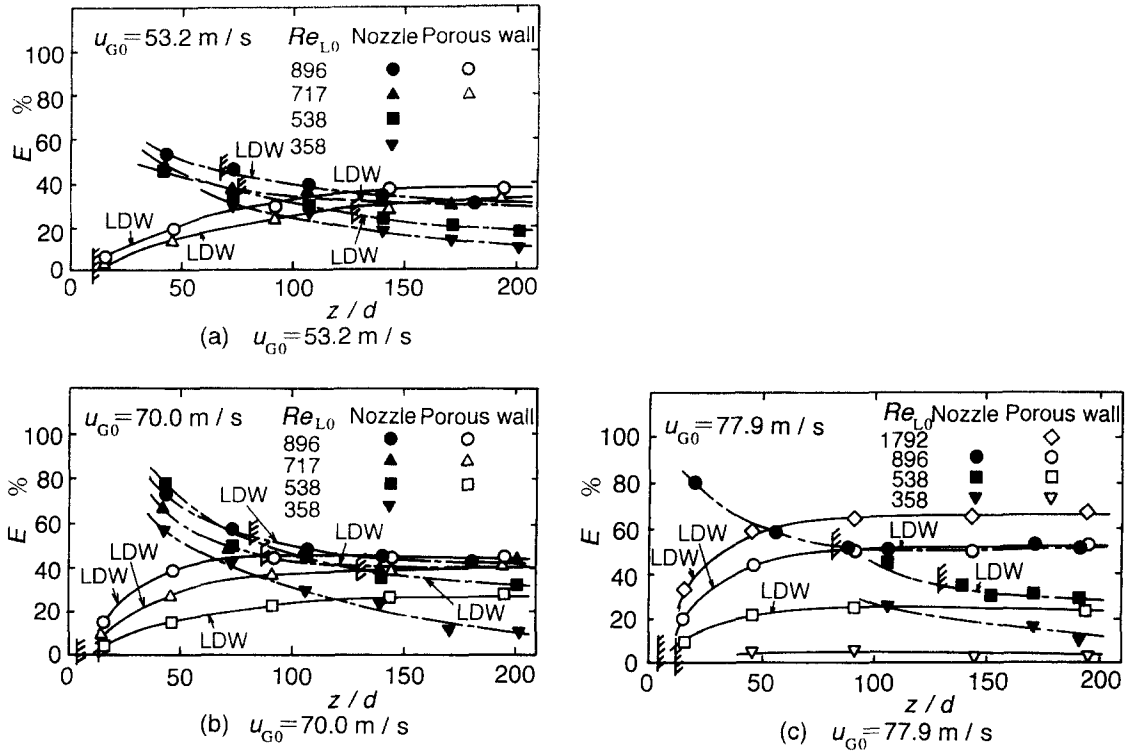

Figure 16. Axial change in the fraction of liquid entrained E: (a) $u_{G0} = 53.2$ m/s; (b) $u_{G0} = 70.0$ m/s; (c) $u_{G0} = 77.9$ m/s. Oblique lines show the inception points of LDW. LDW appear downstream of the inception points. As Re_{L0} increases, LDW appear farther upstream. The solid lines show the data for porous wall mixing; and dashed lines show the data for nozzle mixing.

of the structure of the liquid film in an annular mist flow. Therefore, wave velocities and frequencies at these conditions should be viewed with some caution.

3.5. Entrained water mass flux

It is important to know how the flow regime changes with u_{G0}, u_{L0} and z/d, in order to understand the developing flow mechanism in an annular mist flow. It has been clarified previously, for a downward annular mist flow in a vertical pipe, that it was more precise to define the length of the non-equilibrium region by the distributions of the entrained water mass flux than by any other factor, e.g. pressure loss (Takahama *et al.* 1980). In the present work, the radial distributions of entrained water mass flux G_{en} (Kg/m^{2}s) were measured by the same method as used in the previous report (Takahama *et al.* 1980).

Figure 15 shows typical examples of the axial change in the distributions of G_{en} in both mixing methods, where r is the radial position to measure droplets and R is the pipe radius. In porous wall mixing [figure 15(a)], the value of G_{en} is a minimum in the center of the pipe and increases toward the pipe wall near the mixing device. The radial distributions of G_{en} become more uniform and the value of G_{en} increases axially. Finally, the G_{en} distributions become constant at a certain z/d. On the other hand, in nozzle mixing, the G_{en} distributions are in a marked contrast [figure 15(b)]: G_{en} is a maximum in the center of the pipe and decreases toward the pipe wall; the G_{en} distributions decrease and become more uniform in the axial direction, and eventually become constant. The distance where G_{en} becomes constant decreases as both u_{G0} and Re_{L0} increase, in either porous wall or nozzle mixing devices.

Next, the total mass flow rate of entrained water droplets per cross section W_{LE} was calculated by a graphic integration using the G_{en} distributions in the radial direction:

$$W_{LE} = \int_A G_{en} dA, \qquad [1]$$

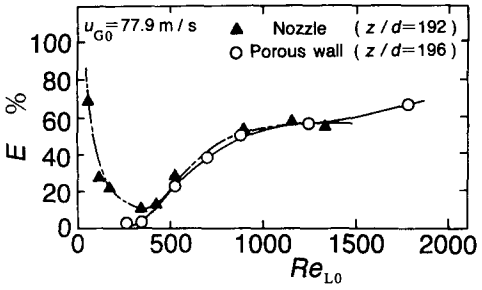

Figure 17. Influence of the mixing method on E.

where A is the cross-sectional area of the pipe. The fraction of liquid entrained E is designated as the ratio of W_{LE} to the mass flow rate of the liquid W_L:

$$E = 100\, W_{LE}/W_L. \qquad [2]$$

E is herewith designated E_S and E_N in the case of porous wall and nozzle mixing, respectively. The length of the non-equilibrium region in annular mist flow $(z/d)_E$ is defined as the distance where E becomes constant, as in the previous report (Takahama *et al.* 1980).

The change in E with distance for the two different inlets shows for what distance the inlet will influence the flow behavior in a two-phase flow. Figure 16 shows the axial changes of the fraction of liquid entrained E in both mixing devices; in figure 16, oblique lines show the inception points of LDW. Figure 16(a) shows the change of E at $u_{G0} = 53.2$ m/s. In porous wall mixing, all measurement points are in flow conditions in which LDW appear. E_S increases gradually as z/d increases at $Re_{L0} = 717$, and becomes almost constant for $z/d \geqslant 150$, at $Re_{L0} = 896$. In nozzle mixing, E_N decreases gradually as z/d increases, and the rate of decrease slows when LDW occur. At $Re_{L0} \leqslant 538$, E_N continues to decrease till $z/d = 200$. At $Re_{L0} \geqslant 717$, E_N almost reaches a constant value. Naturally, $E_N > E_S$ for $z/d \leqslant 100$, and the rate of axial change of E_S and E_N decreases and E_S nearly approaches E_N for $z/d \geqslant 150$. Furthermore, for $z/d \leqslant 100$, E_S abruptly increases with z/d. This shows that the increase in E_S corresponds to the abrupt decrease in the LDW frequency f_d and the flow develops rapidly in this range of z/d.

In the case where the air velocity u_{G0} increases, as shown in figures 16(b) and (c), the LDW do not appear yet at $Re_{L0} = 358$, so $E_N > E_S$, and continues to decrease even for $z/d \leqslant 200$.

At $Re_{L0} = 538$, the LDW appear as clearly shown in figure 6. E_N differs considerably from E_S ($E_N > E_S$). For $z/d \doteqdot 200$, E_N agrees well with E_S [$(z/d)_E \doteqdot 200$]. At $Re_{L0} = 717$ to 896, where the water rate increases further and LDW occur, for $u_{G0} = 70.0$ m/s, $(z/d)_E = 110$ to 140. The value of $(z/d)_E$ decreases as Re_{L0} increases. For $u_{G0} = 77.9$ m/s, $(z/d)_E \doteqdot 90$, E_N almost agrees with E_S. At $Re_{L0} = 1792$, where the water rate increases even more, $(z/d)_E$ tends to decrease considerably; $(z/d)_E \doteqdot 70$ in porous wall mixing. For $u_{G0} = 87.0$ m/s, where the air velocity u_{G0} increases more than ever, $(z/d)_E = 70$ to 80 at $Re_{L0} = 538$ in the case of porous wall mixing. E_S becomes constant ($E_S \doteqdot 0.27$) in the downstream region after $(z/d)_E$, since $(z/d)_E$ becomes rather short as u_{G0} increases [as shown in figure 16(c)]. It was pointed out earlier that there was great non-equilibrium length in the case of porous wall mixing. But these results correspond to the case where either u_{G0} is small or Re_{L0} is low. It is then clear that $(z/d)_E$ decreases considerably, even in porous wall mixing, for the flow condition where u_{G0} is as large and Re_{L0} as high as in this experiment. We suppose that this is due to combined effect of deposition/atomization and wave development.

Additionally, Kulov *et al.* (1979) reported that $(z/d)_E = 48$ to 52 at $u_{G0} = 20$ to 50 m/s and $Re_{L0} = 1700$ to 8500 in a downward flow (25 mm dia). This agrees with our result that $(z/d)_E$ decreases greatly in the case of high u_{G0} and Re_{L0}.

Figure 17 shows the influence of the respective mixing method on E at the position where the flow is fully developed. In nozzle mixing E_N is extremely high, because annular flow is not yet formed on the pipe wall at $Re_{L0} \leqslant 300$. Then E_N abruptly decreases as Re_{L0} increases and has a minimum value at $Re_{L0} \doteqdot 400$. At $Re_{L0} > 400$, E_N begins to increase, but its rate decreases at $Re_{L0} \geqslant 1000$.

On the other hand, in porous wall mixing, E_S begins to increase as the liquid entrainment occurs from the liquid surface at $Re_{L0} \geqslant 250$. Then E_S tends to increase gradually in line with E_N. From figure 17, one sees no difference in the mixing methods: E increases as Re_{L0} increases in both mixing methods, at $Re_{L0} \geqslant 500$, in a fully developed flow with high air velocity.

4. CONCLUSIONS

An experiment was performed on the non-equilibrium region of a downward air–water annular mist flow in a vertical pipe with a porous wall and a central nozzle for supplying liquid. From the observations of the liquid film flow on the pipe wall and measurements of liquid film thickness, wave velocity, frequency and liquid droplet mass flux, the following conclusions were obtained:

(1) With porous wall mixing, LDW occurred farther upstream than in central nozzle mixing. In both cases, LDW occurred farther upstream as u_{L0} increased. With central nozzle mixing, LDW occurred farther downstream as u_{G0} increased.
(2) In nozzle mixing, the maximum and mean liquid film thicknesses t_{max} and t_m increased with the axial distance z/d for $z/d \leqslant 50$, whereas in porous wall mixing no remarkable axial change in t_{max} and t_m was evident.
(3) The radial distribution of the water droplet mass flux G_{en} had a concave shape in porous wall mixing and a convex one in nozzle mixing, near the mixing device. In a fully developed region, the distribution of G_{en} became uniformly flat.
(4) In nozzle mixing, the fraction of liquid entrained E axially decreased monotonously and attained a certain constant value, whereas in the porous wall mixing it increased monotonously and attained a constant value.
(5) For high u_{G0} and high u_{L0}, the non-equilibrium lengths $(z/d)_E$ were 70–140 and were not so remarkably different for either mixing method. The value of $(z/d)_E$ decreased as u_{L0} increased.
(6) There is a critical liquid film thickness that depends heavily on the air velocity in a downward annular mist flow, in contrast with an upward annular mist flow. No matter how the water rate increases, the excess liquid over the critical liquid flow rate is atomized into dispersed water droplets by the force of the air flow.
(7) In porous wall mixing, the velocity of the ripples u_r almost never changes in the axial direction; whereas in nozzle mixing, the velocity u_r axially changes remarkably. Thus, when the air velocity u_{G0} is low, u_r approaches a constant value after decreasing in the flow direction. On the other hand, when u_{G0} is high, u_r becomes constant after increasing in the flow direction, accelerated by high air flow. The tendencies of u_r in both mixing methods coincide for $z/d \geqslant 100$.
(8) The velocity u_d of LDW slightly increases monotonously in the flow direction for both mixing methods.

REFERENCES

FUKANO, T., KAWAKAMI, Y., ITOH, A. & TOMINAGA, A. 1987 Mechanism of the disturbance wave generation in a vertical up- and downward gas–liquid two-phase annular flow. *Trans. JSME* **53B,** 2982–2989. In Japanese.

JAYANTI, S. & HEWITT, G. F. 1991 Structure of interfacial waves in air–water horizontal annular flow. In *Phase–Interface Phenomena in Multiphase Flow*, pp. 95–104. Hemisphere, New York.

KULOV, N. N., MAKSIMOV, V. V., MALJUSOV, V. A. & ZHAVORONKOV, N. M. 1979 Pressure drop, mean film thickness and entrainment in downward two-phase flow. *Chem. Engng. J.* **18,** 183–188.

NEDDERMAN, R. M. & SHEARER, C. J. 1963 The motion and frequency of large disturbance waves in annular two-phase flow of air–water mixtures. *Chem. Engng. Sci.* **18,** 661–670.

OKADA, O. & FUJITA, H. 1990 Experimental studies of annular-mist flow in the non-equilibrium region of a long horizontal pipe (comparison between the mixing methods by a nozzle and a porous wall). In *Proc. Int. Symp. on Gas–Liquid Two-phase Flows, ASME Winter A. Mtg*, Dallas, TX, pp. 57–64.

SAKAGUCHI, T., AKAGAWA, K., HAMAGUCHI, A. & IMIYA, K. 1979 Wave structure of liquid–gas two-phase annular flow in a vertical tube. In *Proc. 16th Natn. Heat Transfer Symp. of Japan, Hiroshima*, pp. 121–123. In Japanese.

SEKOGUCHI, K., NISHIKAWA, K., NAKASATOMI, M., NISHI, H. & KANEUZI, A. 1973 Liquid film flow phenomena in upwards two-phase annular flow. *Trans. JSME* **39,** 313–323. In Japanese.

SEKOGUCHI, K., TANAKA, O., UENO, T., HURUKAWA, T., EZAKI, S. & NAKASATOMI, M. 1983 An investigation of the flow characteristics in the disturbance wave region of annular flow (1st Report: effect of tube diameter). *Trans. JSME* **49B,** 395–405. In Japanese.

TAKAHAMA, H., OKADA, O. & HAMADA, Y. 1980 Study on annular mist flow in pipe (1st Report: investigation of the non-equilibrium length and changes of some factors in the non-equilibrium region). *Bull. JSME* **23,** 1849–1856.

TAKAHAMA, H., OKADA, O., FUJITA, H. & MIZUNO, A. 1983 Study on annular mist flow in pipe (2nd Report: Behavior of water film in the non-equilibrium region of downward annular mist flow with low water flow rate). *Bull. JSME* **26,** 2091–2099.

WEBB, D. R. 1970 Studies of the characteristics of downward annular two-phase flow. Part 1: the effect of length. Report AERE-R6426, pp. 1–48.

WOODMANSEE, D. E. & HANRATTY, T. J. 1969 Mechanism for the removal of droplets from a liquid surface by a parallel air flow. *Chem. Engng. Sci.* **24,** 299–307.